

## Study of nuclear shapes in Tl isotopes via excited state giant dipole resonance studies in the reaction $^{16}\text{O} + ^{181}\text{Tl}$

D. R. Chakrabarty, V. M. Datar, R. K. Choudhury, and B. K. Nayak  
*Nuclear Physics Division, Bhabha Atomic Research Centre, Bombay 400 085, India*

Y. K. Agarwal, C. V. K. Baba, and M. K. Sharan\*  
*Tata Institute of Fundamental Research, Homi Bhabha Road, Colaba, Bombay 400 005, India*

(Received 31 January 1996)

The present paper describes the measurement of high energy gamma rays ( $\sim 5\text{--}22$  MeV) in the reaction  $^{16}\text{O} + ^{181}\text{Tl}$ . Singles measurements were performed at  $E(^{16}\text{O})=84, 89,$  and  $107$  MeV and the multiplicity gated measurements along with the angular distributions were made at  $E(^{16}\text{O})=94$  MeV. It is seen that the Tl nuclei are nonspherical at the excitation energies and spins relevant for the present work. The angular distribution data can be explained only by incorporating large orientation fluctuations. An attempt has been made to extract information on shape fluctuations directly from the  $\gamma$  spectra. Under the restriction of using a common ‘‘intrinsic’’ strength function characterized by  $E_0$  and  $\Gamma_0$  for the multiplicity gated data sets, a small increase of the effective mean deformation and a drive towards triaxiality ( $\gamma \sim 30^\circ$ ) with angular momentum is brought out. If this restriction is relaxed, however, the data can be understood also with a smaller value of  $\gamma$ . The singles data can be understood within the same framework with a higher value of  $\Gamma_0$ . [S0556-2813(96)03906-4]

PACS number(s): 24.30.Cz, 24.60.Dr, 25.70.Gh, 27.80.+w

### I. INTRODUCTION

Soon after the first experimental observation of the giant dipole resonance (GDR) built on excited states in the heavy ion fusion reactions [1], a series of experiments were reported [2,3] on the extraction of nuclear shape information at high spin and nonzero temperature from the excited state GDR studies. It was later realized that it is rather difficult to extract this information from such studies in an unambiguous manner. The main reason is that at high excitation energies and spins, the nuclei may not attain a unique shape and/or orientation with respect to the spin axis. These shape and orientation fluctuations lead to difficulties in the unambiguous unfolding of experimental data. Moreover, even for a unique deformed shape with axially symmetric deformation, knowledge of the ratio of the widths of the two characteristic components of the GDR is necessary to extract the sign of deformation, i.e., the prolate or the oblate character. The angular distribution can be of more help but again the general behavior of the energy dependence of the angular anisotropy is almost similar for, say, the collective prolate and the non-collective oblate shapes. If the ground state systematics of the GDR strength function for the deformed nuclei is taken as a guide, then the width of the higher energy component should be more than that of the lower one. This has also been justified by some theoretical calculations [4]. With such a hypothesis experiments on the Pb isotopes ( $A \sim 200$ ) revealed [5,6] a spherical to prolate shape transition at a spin value of  $14\hbar$  to  $18\hbar$ . It was mentioned in that work that the shape transition is a general feature in this mass region and is

not sensitively dependent on neutron number. The present work reports on the study of the GDR built on excited states in the Tl isotopes ( $A \sim 200$ ). The motivation is to investigate the generality of the shape transition phenomenon in a different element in this mass region and to make more exclusive measurements on the spin dependence of this phenomenon.

Another relevant question is regarding the width increase of the GDR as a function of temperature and spin. It is generally believed [3] that the GDR width increases at high excitation energies due to the increased shape fluctuation at higher temperature and angular momenta and the convolution of the strength function over different shapes. The inherent increase in damping width with excitation energy is predicted to be small [7]. The above ideas together with theoretical calculations of the free energy surfaces of nuclei have been used in the analyses of some experimental data [3,8]. Although the fits to the data are not always very good, it is claimed that this model of the GDR width increase is supported by the data. A systematic investigation of this aspect is therefore necessary in other systems. The present work addresses these aspects also in the  $A \sim 200$  region for nuclei with nearly spherical ground state shapes. The attempt here is to extract information on shape fluctuations directly from the data and not to test any theoretical energy surface calculations.

### II. EXPERIMENTAL METHODS

The experiments were carried out at the 14UD Pelletron accelerator laboratory at Bombay using  $^{16}\text{O}$  beams bombarding a self-supporting rolled target ( $\sim 2$  mg/cm<sup>2</sup>) of natural tantalum. The measurements consisted of three parts. In the first part, the singles gamma ray spectra were measured at three beam energies of  $\sim 84, 89,$  and  $107$  MeV. High energy

\*Present address: Department of Physics, SUNY, Stony Brook, NY 11794.

gamma (HEG) rays in the energy range of  $\sim 5\text{--}22$  MeV were detected in an array of seven 15 cm thick, closely packed regular hexagonal NaI(Tl) detectors, each inscribed in a circle of 7.5 cm radius. The front face was covered with a 5 mm thick lead sheet to cut down the low energy  $\gamma$  rays and x rays produced in the target by beam bombardment. The detector assembly was placed at  $90^\circ$  and at distances of 50–100 cm in various runs. The other details of the detector assembly including the measurements of the response function, energy calibration, associated electronics, etc., are described elsewhere [9,10]. The HEG rays were detected in coincidence with a BaF<sub>2</sub> detector (5 cm diameter  $\times$  7.6 cm length) situated at  $\sim 6$  cm from the target. The reduction of the cosmic ray events through this coincidence requirement was estimated to be sufficient in the energy range of interest and no further active or passive shield for cosmic rays was used. The BaF<sub>2</sub> detector also served as a trigger detector for the time of flight (TOF) measurement and subsequent neutron-gamma discrimination. Also the coincidence requirement with this detector of a geometrical efficiency of  $\sim 4\%$  emphasized the high multiplicity and, hence, fusion events in these measurements. The reduction of the pileup events was achieved through the pulse shape discrimination method with a hardware gate on the nonpileup condition [9,10]. The data were recorded in a PC-based CAMAC system as two-dimensional spectra of energy deposited in the HEG detector versus TOF. Typical time resolution was  $\sim 3$  ns.

For a more exclusive measurement on the spin dependence of the excited state GDR decay, the second part of the experiment consisted of measuring HEG rays in the same reaction in coincidence with a multiplicity detector assembly. The beam energy in these measurements was  $\sim 94$  MeV. The multiplicity detector assembly consisted of 14 bismuth germanate (BGO) detectors, each 6.3 cm thick and having a regular hexagonal cross section with distance of 5.6 cm between opposite edges. They were close packed in two groups of seven each, facing each other, above and below the target at a distance of  $\sim 1.8$  cm. The middle detector in each group was pulled out to equalize the efficiency of all the detectors. The front faces were covered with cadmium sheets of  $\sim 0.5$  mm thickness. Besides, the 1 mm stainless steel wall of the target chamber almost eliminated the high count rate from the x rays. The efficiencies were measured with a <sup>137</sup>Cs source for 662 keV  $\gamma$  rays kept at the target position. The total efficiency was  $\sim 68\%$ . The HEG detector was kept at  $90^\circ$  and at a distance of 100 cm from the target. The OR of the timing signals from the 14 BGO detectors (after alignment in time) was used to generate the start of a time-to-amplitude converter for the TOF measurement. An analog signal was generated with amplitude proportional to the number of detectors fired in an event and was fed to the analog-to-digital converter (ADC). A pileup parameter was derived from the zero crossover time of the bipolar energy pulse of the HEG detector. The data were recorded in the list mode in a PC-based CAMAC system. For each event the recorded parameters were the energy deposited in the HEG detector, the pileup parameter, the fold or the number of multiplicity detectors fired, and the TOF. The typical time resolution was 4–5 ns for fold  $\geq 3$ .

The third part of the experiment consisted of the measure-

TABLE I. Experimental parameters in the <sup>16</sup>O + <sup>181</sup>Ta reaction at various beam energies. The values of  $E_{\text{beam}}$  are rounded off in the figures, text, and subsequent tables.

$E_{\text{beam}}$ (MeV)	$E_C^x$ (MeV)	$\sigma_{\text{fus}}$ (mb)	$\sigma_{\text{fiss}}$ (mb)	$J_C^{\text{max}}$
83.6	50.4	250	6.8	20
88.7	55.2	510	25.0	30
94.1	60.1	705	90.0	36
106.5	71.6	1100	350.0	49

ment of angular distributions at the beam energy of 94 MeV. The HEG detector was kept at  $45^\circ$ ,  $90^\circ$ , and  $135^\circ$  to the beam at a distance of 100 cm. The measurements were made in coincidence with another multiplicity detector setup consisting of eight regular hexagonal NaI(Tl) detectors, each of thickness 7.5 cm and edge-to-edge distance of 5 cm. These were close packed into two groups of four each and kept at a distance of 4 cm from the target. The total efficiency in this case was  $\sim 40\%$ . The data were recorded in the list mode.

Table I lists the beam energies, the mean excitation energies ( $E_C^x$ ) in the compound nucleus (CN), and the fusion and fission cross sections used in the data analysis. The fusion cross sections were extrapolated from the experimental data on the <sup>19</sup>F + <sup>181</sup>Ta reaction [11] and the fission cross sections were obtained from the experimental measurements [12] on the <sup>16</sup>O + <sup>181</sup>Ta system.

### III. EXPERIMENTAL DATA ANALYSIS

#### A. Singles data

The singles  $\gamma$  spectra at the bombarding energies of 84, 89, and 107 MeV were obtained by projecting the energy-dependent ‘‘prompt’’ gated part of the two-dimensional energy versus TOF spectra and subtracting the ‘‘chance’’ gated part. These are shown in Fig. 1. Figure 2 shows the divided plots for the same data. These were derived by dividing the above singles spectra by statistical spectra calculated at the corresponding beam energies with a constant  $E1$  strength (of 0.1 Weisskopf unit). These divided plots are thus representatives of the average  $\gamma$ -ray strength functions  $F(E_\gamma)$  and have been normalized to 1 at  $E_\gamma \sim 7$  MeV [5].

#### B. Multiplicity gated data

From the analysis of the list mode data at the beam energy of 94 MeV, the fold distribution of the multiplicity detectors was extracted for different gamma energy windows set on the HEG detector array. This was done with neutron rejection via the ‘‘prompt’’ condition set on the TOF parameter. The fold distribution showed a distinct difference for the HEG energy below and above  $\sim 8$  MeV. For extracting the multiplicity distribution (of the low energy gamma rays) from these fold distributions, first, the fold response of the BGO array was calculated for different multiplicities with a Monte Carlo computer program. Next, different forms of multiplicity distributions were assumed, the above fold response was convoluted over each, and the resultant fold distributions were compared with the experimental data. The input multiplicity distributions were varied until the best fit to the data was obtained. For HEG above  $\sim 8$  MeV a trian-

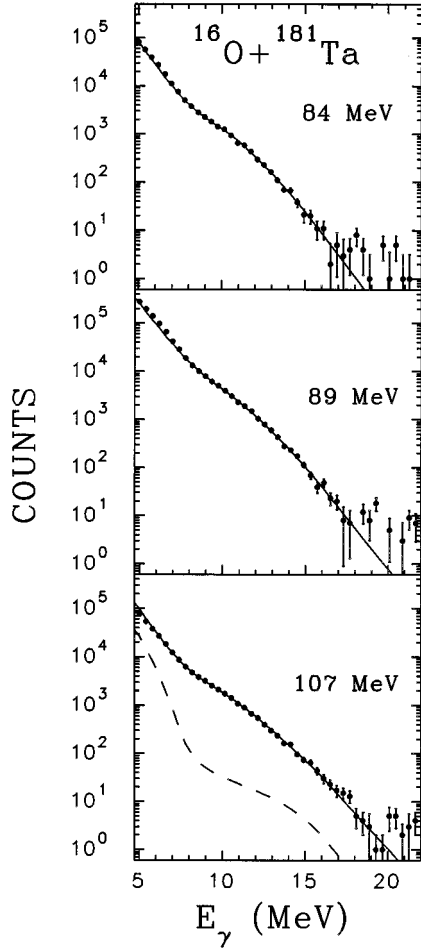


FIG. 1. Singles  $\gamma$ -ray spectra at  $E(^{16}\text{O}) = 84, 89,$  and  $107$  MeV. Also shown are the best prolate fits (solid lines) and the calculated fission fragment contribution at the highest energy (dashed line).

gular multiplicity distribution with a diffuse falloff, characterized by two parameters  $M_{\text{max}}$  and  $\delta M$  in

$$P(M) = \frac{(2M+1)}{1 + \exp[(M - M_{\text{max}})/\delta M]}$$

was found to give the best fit to the data. These fits along with the experimental fold distributions are shown in Fig. 3. For HEG below  $\sim 8$  MeV (Fig. 4) it was not possible to fit the data with a single component multiplicity distribution. A low multiplicity component with a Gaussian distribution [mean  $\sim 3.7$  and full width at half maximum (FWHM) of  $\sim 3.3$ ] was added to get the fits. The relative intensity of the second component for different HEG windows is shown in Fig. 5. The peak structure at  $\sim 6$  MeV suggests that a major contribution to this component arises from the inelastic scattering or transfer reaction in the  $^{16}\text{O} + ^{181}\text{Ta}$  system. Figure 6 shows the best fit parameters  $M_{\text{max}}$  and  $\delta M$  of the main component for different HEG windows. A slight reduction of  $M_{\text{max}}$  at higher gamma energies might be due to the fact that higher energy gamma rays originate relatively more from the lower angular momentum states of the compound nucleus. The  $\delta M$  parameter is practically independent of the  $\gamma$ -ray energy.

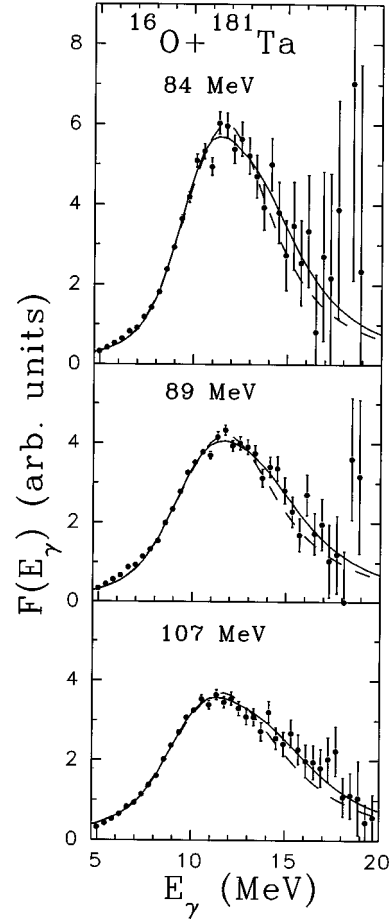


FIG. 2. Divided plots of the singles  $\gamma$ -ray spectra at  $E(^{16}\text{O}) = 84, 89,$  and  $107$  MeV. Also shown are the best prolate (solid lines) and spherical (dashed lines) fits.

It is now possible to invert the problem and derive the multiplicity windows corresponding to different fold windows. Only the main component of the  $M$  distribution is considered. It should be noted that the emphasis of the subsequent data analysis will be on the HEG region above 8 MeV in which the other component is anyway not present. The average value of the multiplicity for different fold windows has very small variation with  $\gamma$ -ray energy. Each fold window actually corresponds to an accepted multiplicity distribution. For the fold windows of 3–4, 5–6, and 7–14, the average values are  $\sim 7.1, 10.4,$  and  $15.5$  and FWHM's are  $\sim 2.8, 3.3,$  and  $5.0,$  respectively. We have used these three fold windows in our subsequent discussion on the spin dependence of the  $\gamma$ -ray spectra which are shown in Fig. 7 (after eliminating the neutron-induced events). For  $E_\gamma < 8$  MeV only the yields corresponding to the main component of the multiplicity distribution (due to fusion) are plotted. These were obtained from the measured yield after subtracting the intensity of the second component in different fold windows. Figure 8 shows the corresponding divided plots of the three spectra.

### C. Angular distribution data

In the analysis of the angular distribution data at the beam energy of 94 MeV, a fold gate  $\geq 2$  was employed in the

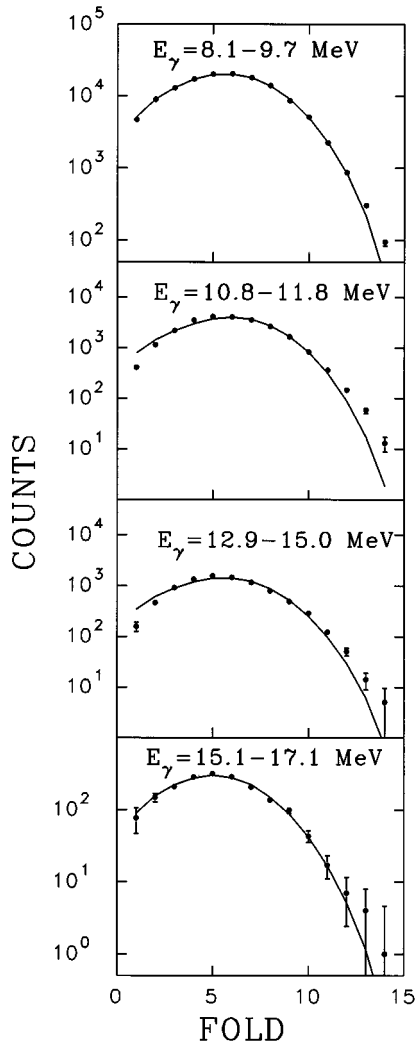


FIG. 3. Experimental fold distributions and the best fits (solid lines) for different  $E_\gamma$  bins with  $E_\gamma > 8$  MeV.

software. This was used basically to emphasize the fusion events. Since the measured anisotropy was small, the pileup correction was applied with special care as described in the following. The pileup spectra were created for different energy windows with a ‘prompt’ condition on the TOF parameter. In a given window on the pileup parameter set around the peak of the spectrum, there are also events due to pileup, the fraction of which can be calculated from the extrapolation of the pileup tail into the peak region. This needs a subtractive correction. The accepted window also may be narrower than what it should be and this needs an additive correction. For each  $\gamma$ -ray energy window the total correction factor was calculated from a careful inspection of the pileup spectra. This energy-dependent correction was finally applied to the  $\gamma$ -ray spectrum obtained by subtracting the ‘chance’ gated energy spectrum from the ‘prompt’ gated one with a window set on the pileup parameter around the peak region. This way the  $\gamma$ -ray energy spectra were generated for each angle.

Before taking the ratio of the yields at  $45^\circ$  or  $135^\circ$  to that at  $90^\circ$  (we shall define the average of these two ratios as the anisotropy parameter) the contribution from the Doppler ef-

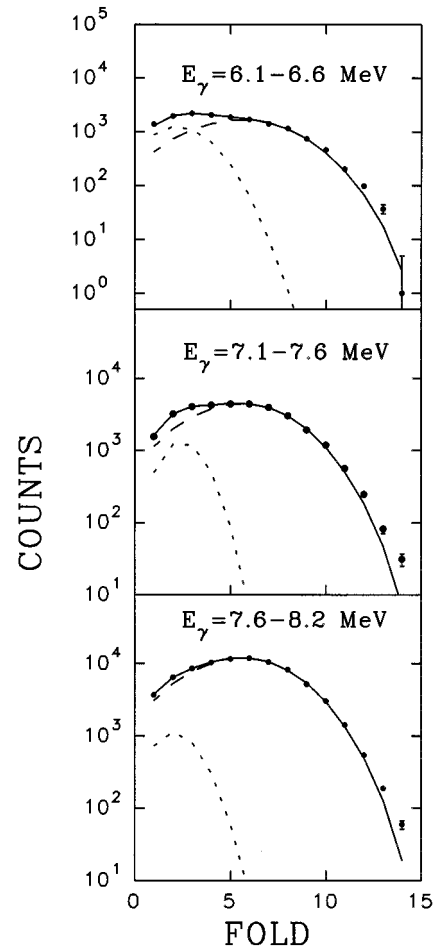


FIG. 4. Experimental fold distributions and the best fits for different  $E_\gamma$  bins with  $E_\gamma < 8$  MeV. The main component and the low multiplicity component (see text) of the fits are shown by the dashed and dotted lines, respectively.

fect was corrected for. This was done in the following way. First a statistical model spectrum was calculated incorporating the GDR parameters which reasonably explains the data at  $90^\circ$  and Doppler-corrected spectra were generated at  $45^\circ$  and  $135^\circ$  in the laboratory. The change in the correction factors arising due to the spectrum folding by the response function of the detector was estimated to be less than 0.5%.

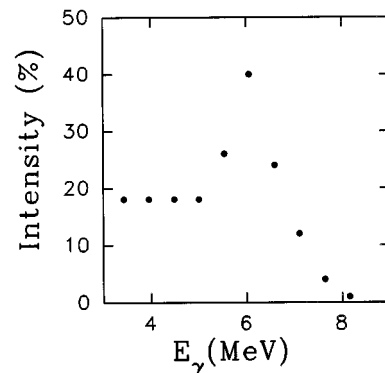


FIG. 5. Relative intensity of the low multiplicity component for different  $E_\gamma$  bins.

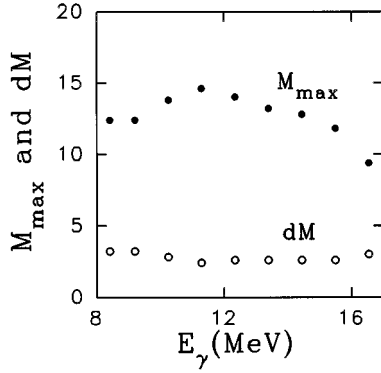


FIG. 6. Best fit  $M_{\max}$  and  $\delta M$  for different  $E_{\gamma}$  bins.

From the ratio of these calculated spectra at  $45^{\circ}$  and  $135^{\circ}$  to that at  $90^{\circ}$ , the energy-dependent Doppler correction factors were estimated. These varied from  $\sim 3\%$  to  $10\%$  in the range of 7–17 MeV. These correction factors were then applied to the  $45^{\circ}$  and  $135^{\circ}$  data before taking the ratio with the  $90^{\circ}$  data. The ratios  $W(45^{\circ})/W(90^{\circ})$  and  $W(135^{\circ})/W(90^{\circ})$  agreed with each other to within 3% for the  $\gamma$ -ray energy range of 8–17 MeV. These ratios were averaged to derive

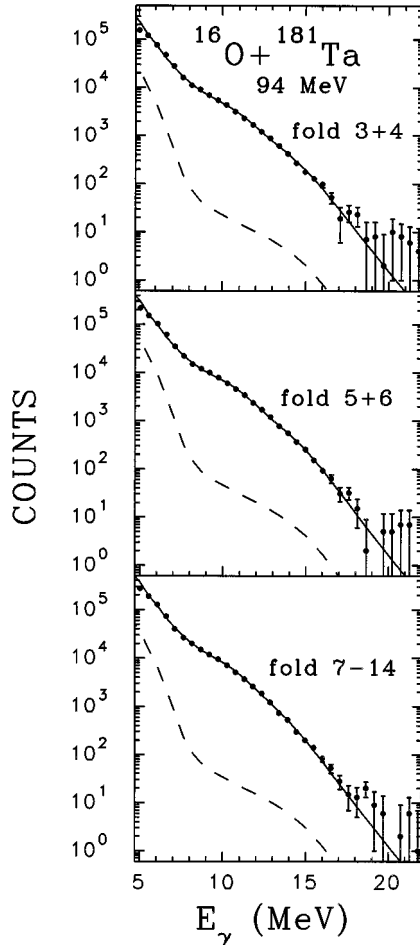


FIG. 7. Fold gated  $\gamma$ -ray yields for the three different fold windows. Also shown are the best prolate fits (solid lines) and the calculated fission fragment contributions (dashed lines).

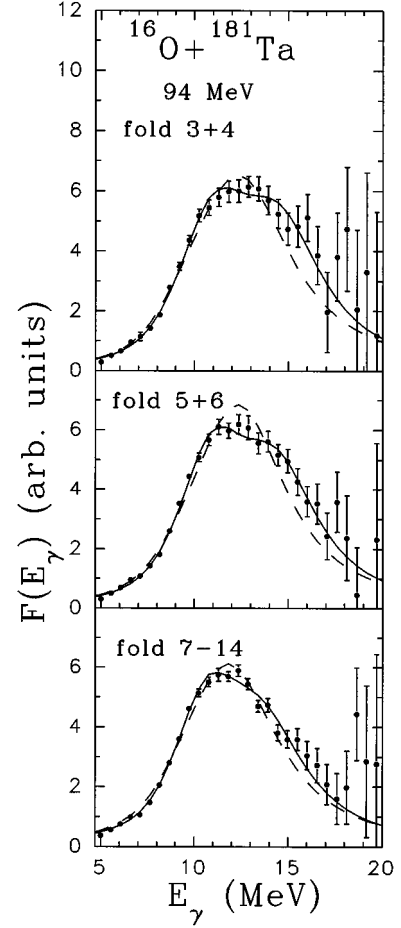


FIG. 8. Divided plots of the  $\gamma$ -ray spectra for the three different fold windows. Also shown are the best prolate (solid lines) and spherical (dashed lines) fits.

the anisotropy parameter as a function of  $E_{\gamma}$  and are shown in Fig. 9.

#### IV. STATISTICAL MODEL ANALYSIS

The measured  $\gamma$ -ray spectra for different beam energies and fold windows show the well-established GDR bumps

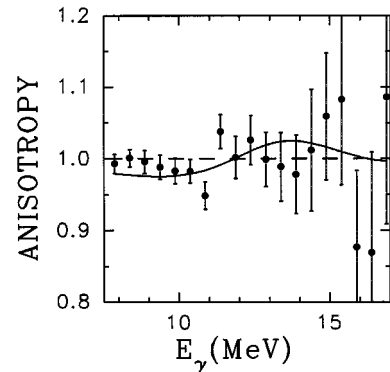


FIG. 9. Angular anisotropy as a function of the  $\gamma$ -ray energy. The calculated anisotropy (solid line) is with the parameters  $\beta_0=0.0$ ,  $\Delta\beta=0.16$ ,  $\gamma_0=4^{\circ}$ ,  $\Delta\gamma=12^{\circ}$ ,  $\xi_0=0.0$ ,  $\Delta\xi=0.7$ ,  $\phi_0=0.0$ ,  $\Delta\phi=0.0$ ,  $E_0=13.8$  MeV,  $\Gamma_0=4.5$  MeV, and  $\delta=1.5$ . The dashed line corresponds to isotropic distribution.

TABLE II. Best fit parameters for spherical, prolate, and oblate fits to the singles and multiplicity gated spectra. 94A, 94B, 94C refer to the fold windows 3–4, 5–6, 7–14, respectively, for the 94.1 MeV data. All energies are in MeV. Errors in  $E_1$ ,  $\Gamma_1$ ,  $E_2$ , and  $\Gamma_2$  are less than 0.2, 0.5, 0.7, and 0.7 MeV, respectively, for prolate fits. The  $\chi^2$ 's are calculated for 23 and 17 fit points for the singles and multiplicity gated data, respectively.

$E_{\text{beam}}$	Spherical		Prolate			Oblate		$\chi^2$
	$E_D/\Gamma_D$	$\chi^2$	$E_1/\Gamma_1$	$E_2/\Gamma_2$	$\chi^2$	$E_1/\Gamma_1$	$E_2/\Gamma_2$	
84	12.6/5.8	29	11.4/4.0	14.2/6.2	21.0	11.8/5.1	14.3/4.4	24.6
89	12.8/6.8	60	11.5/5.0	14.4/7.0	34.9	12.1/5.8	15.8/5.2	40.2
107	12.8/7.5	41	11.4/5.1	14.8/8.0	15.4	11.8/5.9	16.0/4.4	14.6
94A	13.4/6.5	46	11.7/3.9	15.4/5.4	12.6	12.3/5.2	15.8/2.7	20.7
94B	13.3/5.8	110	11.6/3.5	15.2/5.2	18.2	12.2/4.4	15.7/2.4	31.3
94C	12.8/6.0	66	11.3/3.5	14.4/5.5	19.4	11.9/4.6	15.4/3.4	28.3

and the GDR strength function was extracted for the various cases through the statistical model calculations using the code CASCADE [13]. In these calculations the angular momentum distribution of the CN population was taken as

$$P(J_C) = \frac{(2J_C + 1)}{1 + \exp[(J_C - J_C^{\text{max}})/\delta J]},$$

with  $\delta J = 2$ , and  $J_C^{\text{max}}$  consistent with the input fusion cross sections. In the singles experiments the data were collected in coincidence with a BaF<sub>2</sub> detector of total efficiency  $\sim 3\%$ . This condition biased the data to higher angular momenta in the CN and a direct comparison of the normal CASCADE calculation may not be justified. However, even for the lowest beam energy where the effect should be maximum, it was estimated to be insignificant. To examine this, we calculated the  $\gamma$ -ray spectrum at this beam energy by taking the entire population ( $J_C = 0$  to  $\sim 25$ ) and by restricting the CN population from  $J_C = 15$ – $25$ . The change in the chi square of the fit to the data was less than 8%.

An important point to consider in the calculation of the gamma spectra in the present case is the contribution from the excited fission fragments. This has been estimated from a detailed calculation considering (1) the fragment mass and charge distribution [14,15], (2) the excitation energy distribution in the fragments obtained from the CN excitation energy distribution at each step of decay and the kinetic energy distribution of the fragments with the mean obtained from the Viola systematics [16], (3) the spin distribution in the fragments [17,18], and (4) the GDR built on excited states (we used mean energy 16 MeV and width 5.5 MeV). The contribution from the fission fragments is found to be most important at the highest beam energy of 107 MeV which is shown in Fig. 1 after folding over the response function of the detector. Beyond  $E_\gamma \sim 7$  MeV it is less than  $\sim 6\%$ , the highest contribution being at  $\sim 16$  MeV where the GDR strength function has a maximum for the fragments. The contribution from fission fragments is less important at 94 MeV bombarding energy. In the fold gated data, the fractional contribution in the fold windows 3–4, 5–6, and 7–14 were taken as 20%, 40%, and 35%, respectively, of the total fission fragment yield. These estimates were based on the fold response of the multiplicity setup and the multiplicity distribution of low energy gamma rays from the fission fragments. The calculated fission spectra (after folding) are

shown for each fold window in Fig. 7. The fission fragment contribution at still lower bombarding energies was neglected.

For the extraction of the GDR strength function at different bombarding energies, it is parametrized as either one or two component Lorentzians, viz.,

$$F_L(E_\gamma) = \frac{\Gamma^2 E_\gamma^2}{(E_\gamma^2 - E_R^2)^2 + \Gamma^2 E_\gamma^2},$$

where  $E_R$  and  $\Gamma$  are the energy and width parameters. It is generally true that one component corresponds to a spherical shape and two components to a deformed shape of the nuclei. The CASCADE calculations were made for different energy and width parameters of the GDR and the resulting  $\gamma$  spectrum was folded with the detector response function and compared with the data. For the 107 MeV and 94 MeV bombarding energies, the fission fragment  $\gamma$  contributions (discussed above) were added. In all the calculations the total sum rule strength of 100% was used. For the one (two) component fits to the data there were two (four) free parameters corresponding to the GDR energy and width. For the two component fits the relative strengths of the low and high energy components were fixed at 1:2 (prolate) or 2:1 (oblate). The nuclear level density was calculated with the prescription of Ignatyuk *et al.* [19] as elaborated in [20]. Figure 2 shows the best fits obtained to the singles data at different energies using one (dashed curve) and two (solid curve) component Lorentzians. In Fig. 1, only the prolate fits are shown. The GDR parameters corresponding to the best fits for spherical, prolate, and oblate fits are given in Table II.  $E_D$  and  $\Gamma_D$  are GDR energy and width for the spherical (one component) fit and  $E_1, E_2$  and  $\Gamma_1, \Gamma_2$  are the energies and widths of lower and upper components in the prolate-oblate (two component) fits. The chi squares were calculated for the fit region of gamma energy between 8 and 17 MeV.

Before discussing the CASCADE calculations for the fold gated data it is necessary to know the spin windows in the CN corresponding to different fold windows. The calculations were done with sharp limits for these spin windows, although in reality it is not so. This, however, should lead to insignificant error in the extracted GDR parameters. The limits on CN spins for the three fold windows mentioned earlier were estimated in the following manner. From the experimentally extracted multiplicity distribution, the fractions of

total evaporation cross section in the fold windows 3–4, 5–6, and 7–14 were first calculated to be 22%, 30%, and 37%, respectively. For the highest fold window the lower limit of the CN spin was then changed until the evaporation cross section became 37% of the total. This lower limit was  $28\hbar$ . The mean spin of the residues (calculated by slightly modifying the code CASCADE) for the CN spin window of  $28\hbar$  and above was estimated to be  $\sim 28\hbar$ . Most of these residues correspond to the  $5n$  ( $\sim 70\%$ ) and  $4n$  channels ( $\sim 30\%$ ). A simultaneous emission of the GDR gamma ray of  $\sim 10$ – $15$  MeV, is expected to lead to the residues  $^{193}\text{Tl}$  and  $^{194}\text{Tl}$ . There are long-lived low lying states in these nuclei with spin  $\frac{9}{2}\hbar$  and  $7\hbar$ , respectively. After subtracting  $\sim 5\hbar$  due to these isomers, assuming an average spin of  $1.6\hbar$  removed per transition, and considering a statistical gamma multiplicity of  $\sim 2$ , the average multiplicity for this CN spin window was estimated to be  $\sim 16$ . This is consistent with the experimentally extracted multiplicity of  $15.5 \pm 5$  in the fold window 7–14. A similar procedure was adopted for the other two fold windows. The CN spin ranges calculated in this way for the three fold windows were  $(11$ – $19)\hbar$ ,  $(20$ – $27)\hbar$ , and  $\geq 28\hbar$ , respectively.

The CASCADE calculations were done for the fold gated data by restricting the CN spin populations in the above ranges. Again both one and two component Lorentzian fits were assumed. The fission fragment  $\gamma$  cross sections were added before folding and comparing with the data. The best spherical and the prolate fits are shown in the divided plots in Fig. 8, as dashed and solid curves, respectively. Figure 7 shows only the prolate fits. The best fit GDR parameters are shown in Table II for spherical, prolate, and oblate fits. The  $\chi^2$  were calculated for the fit region of 8–17 MeV of  $\gamma$ -ray energies.

## V. FLUCTUATION ANALYSES AND DISCUSSION

The GDR parameters fitting the data at different excitation energies and fold windows can be related to (1) the nuclear shape parameters through the Hill-Wheeler relation for GDR energies [3],

$$E_k = E_0 \exp \left[ - \sqrt{\frac{5}{4\pi}} \beta \cos \left( \gamma - \frac{2\pi k}{3} \right) \right],$$

where  $k=1,2,3$  correspond to the  $x,y,z$  axes, respectively, in the intrinsic frame and  $E_0$  is the intrinsic energy of the dipole vibration, and (2) the empirical relation for the width [4],

$$\frac{\Gamma_k}{\Gamma_0} = \left( \frac{E_k}{E_0} \right)^\delta,$$

where  $\Gamma_0$  is the intrinsic width. Here  $\beta$  and  $\gamma$  are the standard deformation parameters [3]. It is clear from Table II that for the oblate solutions the value of  $\delta$  is negative. The ground state systematics for all nuclei shows  $\delta$  to be greater than 1. It has been suggested [4] that  $\delta$  should be  $\sim 1.5$  for the excited state GDR also. Assuming this to be true, the pure oblate solutions can be discarded at once. The spherical solutions can be discarded from the consideration of the goodness of fit, for all data sets except, probably, the 84 MeV one. For the pure prolate solutions the extracted values

TABLE III. Best fit values for  $E_0$ ,  $\Gamma_0$ ,  $\beta$ , and  $\delta$  parameters derived from the prolate fits at each energy/fold. All energies are in MeV.

$E_{\text{beam}}$	$E_0$	$\Gamma_0$	$\beta$	$\delta$
84	13.2	5.4	0.23	2.0
89	13.4	6.3	0.24	1.5
107	13.6	6.9	0.28	1.7
94A	14.1	4.8	0.29	1.2
94B	13.9	4.6	0.29	1.5
94C	13.3	4.7	0.26	1.9

of the  $E_0$ ,  $\Gamma_0$ ,  $\beta$ , and  $\delta$  are shown in Table III for different cases. The  $\beta$  parameter extracted in all cases is large ( $\sim 0.25$ ). While this scenario of pure axially symmetric deformation can explain the data, shape fluctuations are expected to be important at high excitation energies [3,4]. Moreover, as seen in Table III,  $E_0$ ,  $\Gamma_0$ , and  $\delta$  parameters change from case to case. If one believes in the hypothesis that the intrinsic strength function does not change with excitation energy and spin, then all the data sets should be analyzed with the same value of  $E_0$ ,  $\Gamma_0$ , and  $\delta$ , after incorporating the shape and orientation fluctuations. The present approach attempts to extract the mean  $\beta$  and  $\gamma$  directly from the data after incorporating these fluctuations. The point to be noted is that we are not using any theoretical calculations of the energy surfaces and comparing the predictions with our data.

In our analysis, the fluctuation in shape and orientation is described by Gaussian distributions characterized by mean values and FWHM's in  $\beta$ ,  $\gamma$ ,  $\theta$ , and  $\phi$  parameters, where  $\theta$  and  $\phi$  define the orientation of the spin axis. The convention used here is such that for prolate ( $\gamma=0^\circ$ ) and oblate ( $\gamma=60^\circ$ ) shapes the symmetry axes are the  $z$  and  $y$  axes, respectively, and  $\theta$  and  $\phi$  are defined in a conventional manner in this right handed coordinate system. For an assumed set of values of  $E_0$ ,  $\Gamma_0$ , and  $\delta$ , various  $\beta, \gamma, \theta, \phi$  values were selected with a Monte Carlo procedure consistent with the assumed Gaussian distributions. The GDR parameters and the angular anisotropy coefficient  $a_2$  were calculated for each shape and orientation. The angular anisotropy coefficient  $a_2$  for the GDR gamma rays for a certain orientation ( $\theta, \phi$ ) of the spin axis can be shown to be

$$a_2 = \frac{1}{4} [F_x(3 \sin^2 \theta \cos^2 \phi - 1) + F_y(3 \sin^2 \theta \sin^2 \phi - 1) + F_z(3 \cos^2 \theta - 1)].$$

$F_x$ ,  $F_y$ , and  $F_z$  are the relative probabilities for the  $\gamma$  rays to originate from vibrations along the  $x$ ,  $y$ , and  $z$  axes, respectively, which depend on the deformation parameters  $\beta$  and  $\gamma$ . These probabilities are defined as

$$F_x = \frac{f_x}{f_x + f_y + f_z},$$

with

$$f_x \propto \frac{\Gamma_x E_\gamma^4}{(E_\gamma^2 - E_x^2)^2 + \Gamma_x^2 E_\gamma^2}.$$

Here  $E_x$  and  $\Gamma_x$  are the GDR energy and width for vibration along the  $x$  axis.  $F_y, F_z$  are similarly defined.

The energy-dependent  $\gamma$ -ray strength functions at  $90^\circ$  (at which all the spectra were measured) and  $45^\circ$  (another angle in the angular distribution measurements) were calculated from these and averaged over many trials (typically 500–5000) in the Monte Carlo computer program. The volume element in the integration was chosen to be

$$d\tau = \beta^4 \sin 3\gamma d\beta d\gamma d\xi d\phi,$$

as suggested in [4]. Here  $\xi = \cos\theta$ . The average value of any variable  $x$  is defined as  $\langle x \rangle = \int f(x)x d\tau$  where  $f(x)$  is the Gaussian distribution function for  $x$ , i.e.,

$$f(x) \propto \exp\left[-2.77\left(\frac{x-x_0}{\Delta x}\right)^2\right],$$

$x$  standing for the variables appearing in the above volume element. Here  $\Delta x$  is the FWHM of the distribution. The effect due to Coriolis splitting of the strength function was neglected, because it was found to be small.

The resultant strength function at  $90^\circ$  was used in the CASCADE program. The calculated cross sections were folded with the detector response function as mentioned earlier and compared with the data. For comparing with the angular anisotropy data, the strength functions at  $45^\circ$  and  $90^\circ$  were used in the CASCADE calculation, and the ratio was taken after folding with the detector response function. The contributions from fission fragments were justifiably neglected in this case.

The intrinsic GDR energy and width are expected to be similar to those of the ground state GDR strength function. In the mass region of  $A \sim 190$ – $200$  the GDR energies for the spherical cases range from 13.4 to 13.9 MeV and the GDR width from  $\sim 4$  to 5 MeV [21]. In our calculations, we have varied  $E_0$  and  $\Gamma_0$  around these values. For each set of assumed  $E_0, \Gamma_0, \delta$  values the mean and FWHM values of the shape and orientation parameters were varied in different steps until the best fit to the data was obtained for different excitation energies and fold windows. The ranges of  $\beta$  and  $\gamma$  were restricted to  $0$ – $1.0$  and  $0^\circ$ – $60^\circ$ , respectively.

The GDR strength function at a given angle does not change very much with orientation fluctuation, whereas the angular distribution depends both on the shape and orientation fluctuation. We first consider, therefore, the analysis of the angular distribution data, measured at 94 MeV. In the angular distribution measurement the condition of fold  $\geq 2$  was imposed with the eight-detector multiplicity setup (see earlier section). This is equivalent to the fold  $\geq 3$  for the 14-detector multiplicity setup used in spectral measurements. This conclusion was arrived at from the consideration of the multiplicity to fold response of the setups. A consistent description of both angular distribution and spectral measurement at this energy therefore demands simultaneous fits to the angular distribution data and the measured spectrum with a fold window of 3–14. A detailed analysis reveals that it is possible to fit the measured angular anisotropy data either with a large orientation fluctuation or a very large  $\gamma$  fluctuation. The latter possibility can be rejected since this cannot fit the strength function data. In the random selection of the

orientation, the cosine of the angle was randomized to follow the Gaussian distribution. A value of  $\xi_0 = 0$  and a FWHM of at least 0.7 was necessary to describe the data. Note that we have frozen  $\phi_0$  and  $\delta\phi$  to 0.0 in all our calculations. If the nucleus is prolate, then the  $\phi$  fluctuation makes no change in the anisotropy. However, for triaxial and oblate shapes, it is effective. For example, for the pure oblate case and  $\xi_0 = 0, \phi = 0^\circ$  corresponds to the collective rotation and  $\phi = 90^\circ$  to the noncollective rotation around the symmetry axis. It is in principle possible to have combination of  $\theta$  and  $\phi$  fluctuations. Hence it is not easy to extract separate information on the  $\theta$  and  $\phi$  fluctuations, although the  $\theta$  fluctuation is found to be more important for the present data. Figure 9 shows the measured anisotropies and those calculated with the parameters noted in the caption, for different  $E_\gamma$ . We emphasize again that it is not possible to fit the anisotropy data without a large orientation fluctuation. Although the angular distribution is not measured for other cases, we assumed similar orientation fluctuation in all the cases and used the mean value of  $\xi_0 = 0$  and the FWHM = 0.7 in the analyses.

The orientation fluctuation for an axially symmetric deformation can be related to the  $K_0^2$  parameter normally used in fission fragment angular distribution [15] and is given by  $\mathcal{J}_{\text{eff}}T/\hbar^2$  where

$$\frac{1}{\mathcal{J}_{\text{eff}}} = \frac{1}{\mathcal{J}_{\parallel}} - \frac{1}{\mathcal{J}_{\perp}},$$

with  $\mathcal{J}_{\parallel}$  and  $\mathcal{J}_{\perp}$  the moments of inertia parallel and perpendicular to the symmetry axis and  $T$  the nuclear temperature. For the present system at 94 MeV bombarding energy  $K_0^2 \sim 400$  using the rigid body moment of inertia for the prolate shape with  $\beta \sim 0.3$ . This is consistent with the measured near-isotropic angular distribution. A fluctuation towards triaxial shapes would further reduce the anisotropy.

After fixing the  $\theta$  and  $\phi$  distributions, a search for the  $\beta$  and  $\gamma$  distribution was made to find the best fit to the measured spectra at various beam energies and/or fold windows. From the analysis of the multiplicity gated data it was found that it is possible to fit the various sets with the same assumed values of  $E_0, \Gamma_0$ , and  $\delta$ . A choice of  $E_0 = 13.8$  MeV,  $\Gamma_0 = 4.5$  MeV, and  $\delta = 1.5$  provides one such acceptable set. Figure 10 shows the best fits to the data with the relevant parameters listed in Table IV. It should be noted that there is a range of distributions of  $\beta$  and  $\gamma$  characterized by the parameters  $\beta_0, \Delta\beta, \gamma_0$ , and  $\Delta\gamma$ , which can give good fits to the data. For example,  $\beta_0$  can have values between 0.0 and  $\sim 0.2$  for the lowest fold window and between 0.0 and  $\sim 0.27$  for the higher two fold windows. The FWHM's are correspondingly different in such a way that all distributions have very similar average  $\langle\beta\rangle$  within error bars shown in Table IV. Similarly the average  $\langle\gamma\rangle$  lies within the error bars quoted in Table IV, although the distributions can be very different. It is therefore not possible to extract any more detailed information on the nuclear shape fluctuations beyond the average deformation parameters (defined in the manner described above) directly from the data. We can invert this statement to argue that the apparent success of such theories to explain the gamma ray spectra cannot ensure the uniqueness of the calculated energy surfaces. Looking at Table IV for fold gated data we can summarize that  $\langle\beta\rangle$  shows a small increase with fold and, hence, with angular

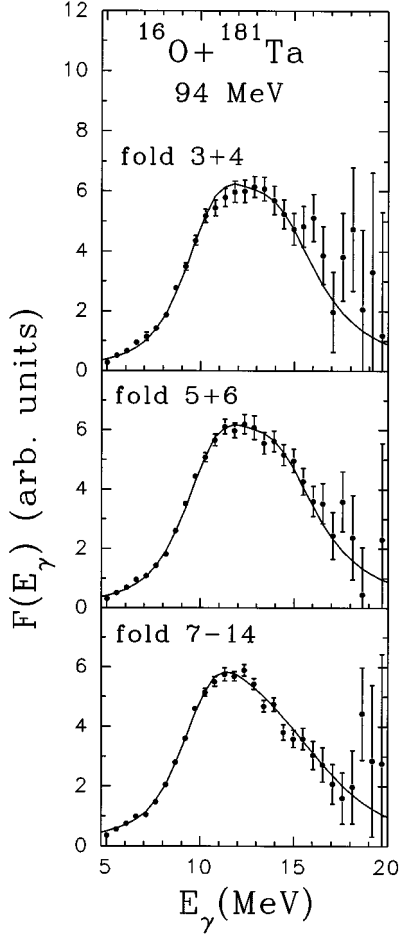


FIG. 10. Divided plots of the  $\gamma$ -ray spectra for different fold windows together with the best fits from fluctuation calculations. The fluctuation parameters are listed in Table IV.

momentum. Also,  $\langle\gamma\rangle$  shows an increase from small values towards  $30^\circ$ , showing that the nucleus tends towards triaxiality at higher spins. It should, however, be kept in mind that if the restriction of same  $E_0$  for all fold windows be relaxed, then the comment on the variation of  $\beta$  and  $\gamma$  will need some modifications. For example, a lower value of  $E_0$  (13.3 MeV) for the higher fold window 7–14 can also fit the data, with the extracted  $\langle\beta\rangle$  being lower ( $0.27 \pm 0.02$ ) and the requirement of triaxiality less stringent ( $\langle\gamma\rangle = 28_{-16}^{+4}$  deg). Finally, the choice of a different value of  $\delta=1.8$  also gives acceptable fits and the overall conclusions about the shape change remain essentially the same.

TABLE IV. Parameters extracted from shape and orientation fluctuation analysis at each energy/fold ratio. All energies are in MeV, and  $\gamma$  is in degrees.  $\xi_0$  and  $\Delta\xi$  are fixed at 0 and 0.7, and  $\phi_0$ ,  $\Delta\phi$  are fixed at  $0^\circ$ .

$E_{\text{beam}}$	$E_0$	$\Gamma_0$	$\langle\beta\rangle$	$\langle\gamma\rangle$	$\chi^2$
84	13.5	5.5	$0.27 \pm 0.04$	$30_{-30}^{+20}$	23
89	13.5	5.5	$0.27_{-0.02}^{+0.04}$	$12_{-12}^{+22}$	31
107	13.5	5.5	$0.31_{-0.02}^{+0.03}$	$15_{-15}^{+17}$	13
94A	13.8	4.5	$0.26 \pm 0.01$	$5_{-5}^{+7}$	14
94B	13.8	4.5	$0.26_{-0.02}^{+0.03}$	$4_{-4}^{+18}$	17
94C	13.8	4.5	$0.34_{-0.02}^{+0.01}$	$31_{-8}^{+2}$	13

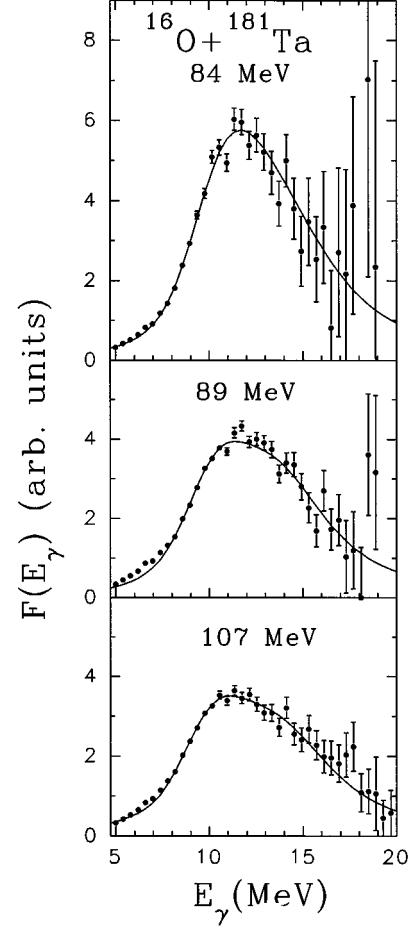


FIG. 11. Divided plots of the  $\gamma$ -ray spectra at  $E(^{16}\text{O}) = 84, 89,$  and  $107$  MeV together with the best fits from fluctuation calculations. The fluctuation parameters are listed in Table IV.

From the fluctuation analysis of the singles data, we find that a common value of  $E_0$  and  $\Gamma_0$  can explain these data sets also. The best fits with the choice of  $E_0=13.5$ ,  $\Gamma_0=5.5$ , and  $\delta=1.5$  (Table IV) are shown in Fig. 11. However, it should be noted that although the same value of  $E_0=13.8$  MeV (used above) is also acceptable in this case, the required value of  $\Gamma_0$  is definitely larger than that used in the multiplicity gated data analysis. It is not clear whether this means a failure of the model or the parameter indeed varies with excitation energy. The uncertainty in the  $\langle\gamma\rangle$  values (Table IV) is too large to derive any conclusion. From

the extracted  $\langle\beta\rangle$  values, again a mild increase at higher bombarding energies cannot be ruled out.

## VI. SUMMARY

In summary, the present paper describes the measurement of high energy  $\gamma$  rays ( $\sim 5$ –22 MeV) in the reaction  $^{16}\text{O} + ^{181}\text{Ta}$  at four bombarding energies. Measurements were made in singles at  $E(^{16}\text{O})=84, 89,$  and  $107$  MeV and in coincidence with a multiplicity setup at  $E(^{16}\text{O})=94$  MeV. The angular distribution measurements were also made at the last beam energy. The data have been analyzed with and without incorporation of fluctuations. The two conclusions that are independent of the method of analysis are (1) the mean deformations needed to explain the  $\gamma$  strength functions are rather large, i.e.,  $\beta\sim 0.25$ , and (2) large orientation fluctuations are needed to explain the observed near isotropy across the GDR region. An attempt has been made to extract information on shape and orientation fluctuations directly from the data, i.e., without incorporating any theoretical predictions based on the calculated energy surfaces in nuclei. Under the restriction of using a common ‘‘intrinsic’’ strength function characterized by  $E_0$  and  $\Gamma_0$  for all the fold gated data sets, the analysis brings out a small increase of the effective mean deformation and a drive towards triaxiality with angular momentum. If this restriction is relaxed, however,

the need for triaxiality is less stringent in the data. It is also possible to explain the singles data sets with a common intrinsic strength function incorporating the shape and orientation fluctuations. The intrinsic  $\Gamma_0$  is, however, larger compared to that in the multiplicity gated data. Finally, there is an ambiguity regarding the details of the shape distributions, and the parameters that can be extracted from such analyses are only the mean values of the shape parameters.

Considering the present data and the earlier measurements on the Pb isotopes, one can deduce that the shape change with spin is a general feature for this mass region. For similar excitation energies, the shape fluctuation for the present case probably is higher. Although no detailed fluctuation analysis for different spin windows is available for Pb isotopes, this opinion can be formed by looking at the slightly increased widths needed to fit the present data in terms of pure prolate hypothesis. A detailed calculation of the energy surfaces for these nuclei would thus be very interesting.

## ACKNOWLEDGMENTS

We thank the Pelletron staff for the smooth running of the accelerator and D. A. Gothe for his help during all stages of the experiment. We also wish to thank Raghav Varma for assistance during some of the early runs.

- 
- [1] J. O. Newton, B. Herskind, R. M. Diamond, E. L. Dines, J. E. Draper, K. H. Lindenberg, C. Schuck, S. Shih, and F. S. Stephens, *Phys. Rev. Lett.* **46**, 1383 (1981).
  - [2] K. A. Snover, *Annu. Rev. Nucl. Part. Sci.* **36**, 545 (1986).
  - [3] J. J. Gaardhoje, *Annu. Rev. Nucl. Part. Sci.* **42**, 483 (1992).
  - [4] Y. Alhassid and B. Bush, *Nucl. Phys.* **A509**, 461 (1990).
  - [5] D. R. Chakrabarty, M. Thoennessen, N. Alamanos, P. Paul, and S. Sen, *Phys. Rev. Lett.* **58**, 1092 (1987).
  - [6] M. Thoennessen, D. R. Chakrabarty, R. Butsch, M. G. Herman, P. Paul, and S. Sen, *Phys. Rev. C* **37**, 1762 (1988).
  - [7] P. F. Bortignon, A. Bracco, D. Brink, and R. A. Broglia, *Phys. Rev. Lett.* **67**, 3360 (1991).
  - [8] A. Bracco *et al.*, *Nucl. Phys.* **A583**, 83 (1995); M. Mattiuzzi *et al.*, *Phys. Lett. B* **364**, 13 (1995).
  - [9] Y. K. Agarwal, C. V. K. Baba, D. R. Chakrabarty, V. M. Datar, D. A. Gothe, H. C. Jain, A. Roy, and M. K. Sharan, *Pramana* **35**, 49 (1990).
  - [10] M. K. Sharan, Y. K. Agarwal, C. V. K. Baba, D. R. Chakrabarty, and V. M. Datar, *Phys. Rev. C* **48**, 2845 (1993).
  - [11] D. J. Hinde, J. R. Leigh, J. O. Newton, W. Galster, and S. Sie, *Nucl. Phys.* **A385**, 109 (1982).
  - [12] F. Videbaek, R. B. Goldstein, L. Grodzins, S. G. Steadman, T. A. Belote, and J. D. Garrett, *Phys. Rev. C* **15**, 954 (1977).
  - [13] F. Puhlhofer, *Nucl. Phys.* **A280**, 267 (1977).
  - [14] F. Plasil, D. S. Burnett, H. C. Britt, and S. G. Thompson, *Phys. Rev.* **142**, 696 (1966).
  - [15] R. Vandenbosch and J. R. Huizenga, *Nuclear Fission* (Academic, New York, 1973).
  - [16] V. E. Viola, K. Kwiatkowski, and M. Walker, *Phys. Rev. C* **31**, 1550 (1985).
  - [17] R. Butsch, M. Thoennessen, D. R. Chakrabarty, M. G. Herman, and P. Paul, *Phys. Rev. C* **41**, 1530 (1990).
  - [18] R. P. Schmitt, L. Cooke, H. Dejbakhsh, D. R. Haenni, T. Shutt, B. K. Srivastava, and H. Utsunomiya, *Nucl. Phys.* **A492**, 130 (1995).
  - [19] A. V. Ignatyuk, G. N. Smirenkin, and A. S. Tishin, *Sov. J. Phys.* **21**, 255 (1975).
  - [20] M. Kicinska-Habior, K. A. Snover, C. A. Gossett, J. A. Behr, G. Feldman, H. K. Glatzel, J. H. Gundlach, and E. F. Garman, *Phys. Rev. C* **36**, 612 (1987).
  - [21] S. S. Dietrich and B. L. Berman, *At. Data Nucl. Data Tables* **38**, 199 (1988).